Formation and exhumation of ultra-high pressure rocks through delamination and mantle upwelling: Evidence from seismic tomographic data beneath the Qinling-Dabie Orogen, Central China

Chuansong He[11], Huili Guo[12] M. Santosh[2, 3]

[1]*Institute of Geophysics, CEA, Beijing 100081, China*

[2]*School of Earth Sciences and Resources, China University of Geosciences Beijing, 29 Xueyuan Road, Beijing 100083, China*

[3]*Department of Earth Sciences, School of Physical Sciences, The University of Adelaide, SA 5005, Australia*

Abstract:

The Qinling-Dabie Orogenic Belt (QDOB) in Central China was built through prolonged subduction-accretion collision events and incorporates many exposures of exhumed ultrahigh-pressure (UHP) metamorphic rocks. We collected a large number of teleseismic and local earthquake data and performed a P-wave tomography and CCP stacking of receiver functions from this region. Our results reveal high-velocity horizontal anomalies at depths of 100-300 km beneath the QDOB, which may be related to the deep subduction or the delamination of the lower crust and lithosphere. We also imaged a low-velocity anomaly at depths of 200-400 km, which may be associated with mantle upwelling in this region. Based on a detailed analysis, we consider that the delamination of the lower crust and lithosphere might have contributed to the formation of the UHP rocks.

Key words: Qinling-Dabie Orogen, ultra-pressure metamorphic rocks, deep subduction, exhumation, tomography, CCP stacking of receiver function.

Plain Language

The Qinling-Dabie Orogenic Belt (QDOB) in Central China is famous in the world due to many exposures of exhumed ultrahigh-pressure metamorphic rocks (UPMR). It is widely accepted that the UPMR may be generated by deep subduction and exhumation. In this study, we collected a large number of teleseismic and local earthquake data and performed a P-wave tomography and CCP stacking of receiver functions in the QDOB. Results reveal high-velocity horizontal anomalies at depths of 100-300 km beneath the QDOB rather than subducted slab-like, the high-velocity horizontal anomalies may be related to the delamination of the lower crust and lithosphere. Based on a detailed analysis, we consider that the delamination of the lower crust and lithosphere might have contributed to the formation of the UHPMRs.

1. Introduction

[1*] Corresponding author. C.S. He (hechuansong@aliyun.com)
[2*] Corresponding author. H.L. Guo (guohuili@live.com)

Ultrahigh-pressure (UHP) metamorphic rocks that carry coesite and diamond inclusions are considered to have formed by the subduction of continental crust to mantle depths of 80-120 km or more in subduction-collision orogens (Chopin, 1984; Deng et al., 2021; Smith, 1984; Sobolev and Shatsky, 1990; Xu et al., 1992). The Qinling-Dabie and its counterpart Sulu orogenic belt in Central China is a classic example for the occurrence of typical UHP rocks, and the orogen was constructed though multi-stage involving subduction-accretion and collision (Zheng et al., 2013; Dong and Santosh, 2016; Dong et al., 2021; Niu, 2021). The final amalgamation of the DQOB involved the collision between the North China Block (NCB) and the South China Block (SCB) during the Early Paleozoic to Early Mesozoic (Chai et al., 2020; Dong and Santosh, 2016; Liu et al., 2016; Wu and Zheng, 2013). Several coesite- and diamond-bearing UHP rocks were reported from this orogenic belt, and have been considered as an indicator for the deep subduction of the continental crust (Deng et al., 2021; Li et al., 2020; Okay et al., 1989; Wang et al., 1989) with one school of thought proposing the subduction of the SCB beneath the NCB during the Triassic (Ames et al., 1996; Hacker et al., 1998; Ma et al., 2021; Yang et al., 2019; Zheng et al., 2005).

Recent geophysical investigations have reported deeply subducted continental crust in the Pyrenees and the Western Alps (Chevrot et al., 2015; Zhao et al., 2015) at depths of 70 km and 75 km. Deep subduction of continental crust has also been identified in the Pamir range (Schneider et al., 2013). However, deeply subducted continental crust has not been unequivocally traced in the QDOB region (Dong et al., 2008; He et al., 2014; Luo et al., 2012) although reflection surveys defined a northward dipping Moho beneath the Dabie region (Wang et al., 2000; Yuan et al., 2003).

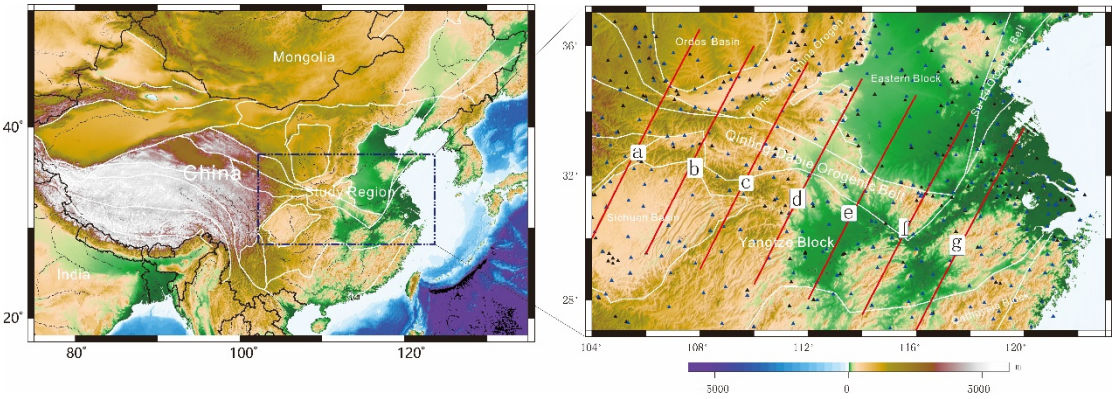

Fig. 1. Left panel: Location of the study region. Right panel: red lines: overlapped profiles of P-wave perturbation and CCP stacking of receiver function, black triangle: seismic station, which record teleseismic events, blue triangle: seismic stations, which record local seismic events. White lines: boundary of geological units.

In order to gain further insights on the deep subduction process, we carried out a P-wave teleseismic tomography and CCP stacking of receiver function study in the QDOB (Fig. 1) by collecting a large number of teleseismic and local earthquake data (teleseism event, see Fig. S1). Our results reveal horizontal lensoid high-velocity anomalies at depth, and low-velocity anomalies in the upper mantle beneath the QDOB, which correlate with delamination and mantle upwelling.

1. **Data**

   (a) **Tomography**

The collected data set included those from permanent seismic stations (316 stations, July 2007-August 2020) and regional seismic network (361 stations, July 1984-July 2018) (Fig. 1). The epicenter distance of the event-station pair for the teleseismic event ranged from 30° to 95°.

The teleseismic waveforms were cut 15 s before and 50 s after the first P-wave arrival from the digital seismogram with bandpass filtering between 0.3 and 3 Hz. The P-wave arrival times were selected from the cut seismograms. The 65449 P-wave arrivals were extracted from the 644 teleseismic events (Fig. S1). Moreover, we also collected a total of 60655 P-wave arrivals from 16862 local earthquakes recorded by 361 seismic stations.

1. **CCP stacking of receiver function**

A total of 1220 teleseismic events were extracted from 316 permanent seismic stations recorded from July 2007 to August 2020 in the study region (Fig. S1). The events were limited to Ms >6.0, and the earthquake epicentral distances ranged from 30° to 90° for individual event-station pairs. A Butterworth bandpass filter between 0.05 and 1 Hz was applied to the raw record, which was cut from 15 s before to 200 s after the P-wave arrival. To obtain a high signal-to-noise ratio for all events, the waveform cross-correlation technique (VanDecar and Crosson, 1990) was used to select consistent raw data. In total, 21627 high-quality receiver functions were calculated by a modified frequency-domain deconvolution with a 1 Hz Gaussian filter and 0.01 water level (Langston, 1979; Zhu and Kanamori, 2000) (for example, please see Fig. S2).

1. **Results**

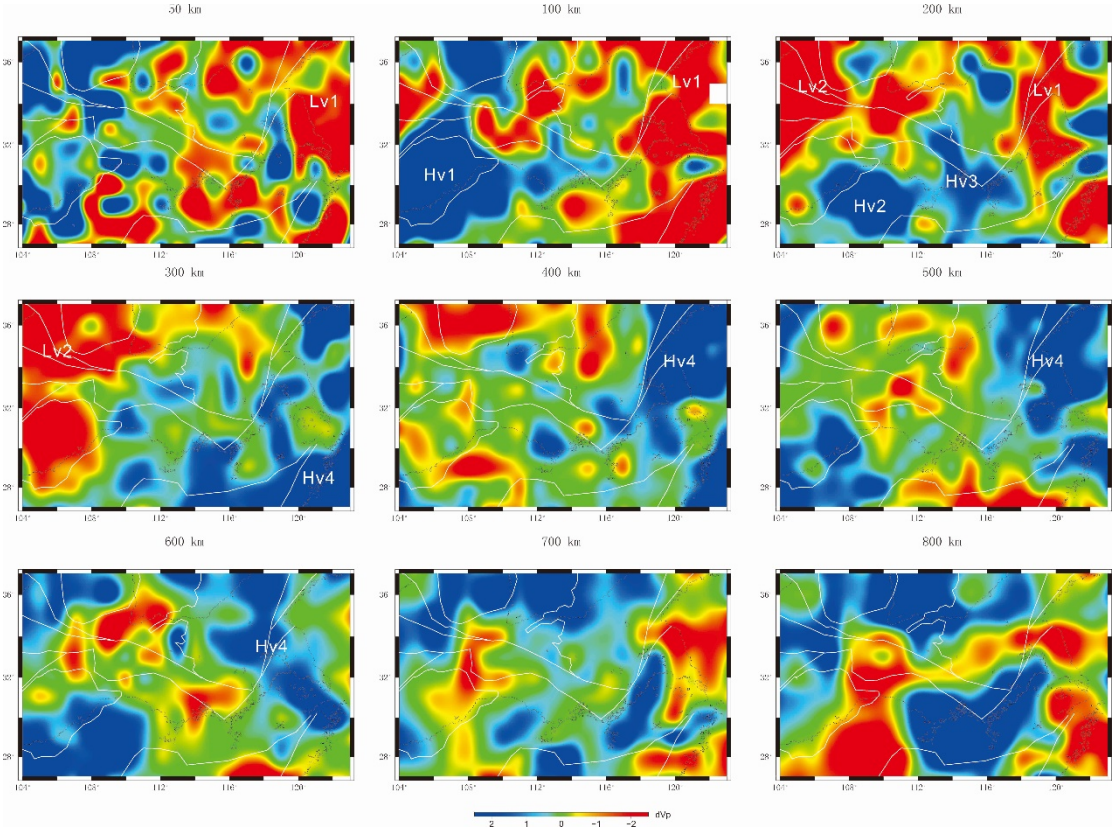

Fig. 2. P-wave perturbation at depth from 50 to 800 km.

Our results show a prominent low-velocity anomaly (Lv1) in the eastern part of the study region (Fig. 2), which is consistent with previous tomographic results (He, 2020; Jiang et al., 2013; Lei, 2012 Tian and Zhao, 2013; Zhao et al., 2012). The high-velocity anomaly (Hv1) at the depth of 100km is interpreted as the lithospheric root beneath the Sichuan Basin (Fig. 2), and previous regional tomography had also defined a similar velocity structure in this area (Li et al., 2006; Shen et al., 2016; Wei et al., 2016). At the depth of 200 km, the high-velocity anomalies (Hv1 and Hv2) appear beneath the Yangtze Block and the Dabie belt respectively (Fig. 2). The low-velocity anomaly (Lv1) beneath the QOB occurs at depths of 200 and 300 km (Fig. 2). Large-scale high-velocity anomaly (Hv4) appears at depths of 300-600 km (Fig. 2). A previous tomography study correlated this high-velocity anomaly with the subducted slab of the Pacific plate in the Mesozoic (He and Zheng, 2018).

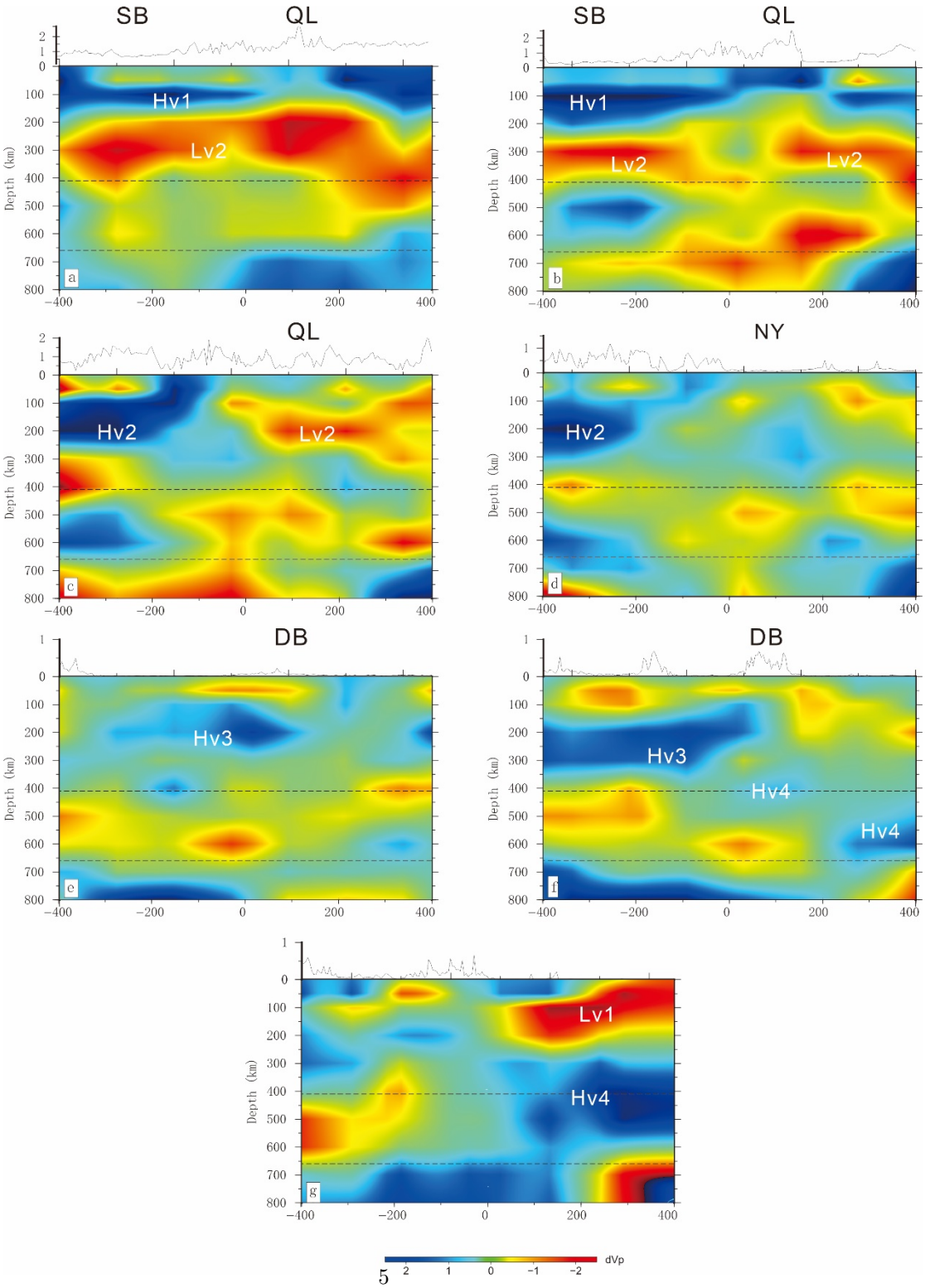
SB
QL
Hv1
Lv2
a
SB
QL
Hv1
Lv2
Lv2
b
QL
Hv2
Lv2
c
NY
Hv2
d
DB
Hv3
e
DB
Hv3
Hv4
Hv4
f
Lv1
Hv4
g
Depth (km)
dVp
2
1
0
−1
−2

Fig. 3. P-wave perturbation profiles (a-g). QL: Orogenic Belt; NY: Nanyang Basin; DB: Dabie Belt; SB: Sichuan Basin.

We also perform 7 profiles of P-wave velocity perturbation which pass through the QDOB (profile location, please see Fig. 1). The results show that the Hv1 is under the Sichuan Basin (Fig. 2a and b). The low-velocity anomaly (Lv2) appears at upper mantle at depths of 200-400 km and is located beneath the QOB (Fig. 2a, b and c). The high-velocity anomaly with the lensoid shape (Hv2) is located at the southern part of the QOB and the Nanyang Basin at depths of 100-300 km (Fig. 2c and d). Another high-velocity anomaly (Hv3) is located at the southern part of the DOB at depths of 150-350 km (Fig. 2e and f). Outside the QDOB, the lens-shaped high-velocity anomaly (Hv4) appears at depths of 300-500 km and is located at the northern part of the f and g profile (Fig. 2f and g). The low-velocity anomaly (Lv1) appears at depths of 0-200 km and is located at the northern part of the g profile (Fig. 2g).

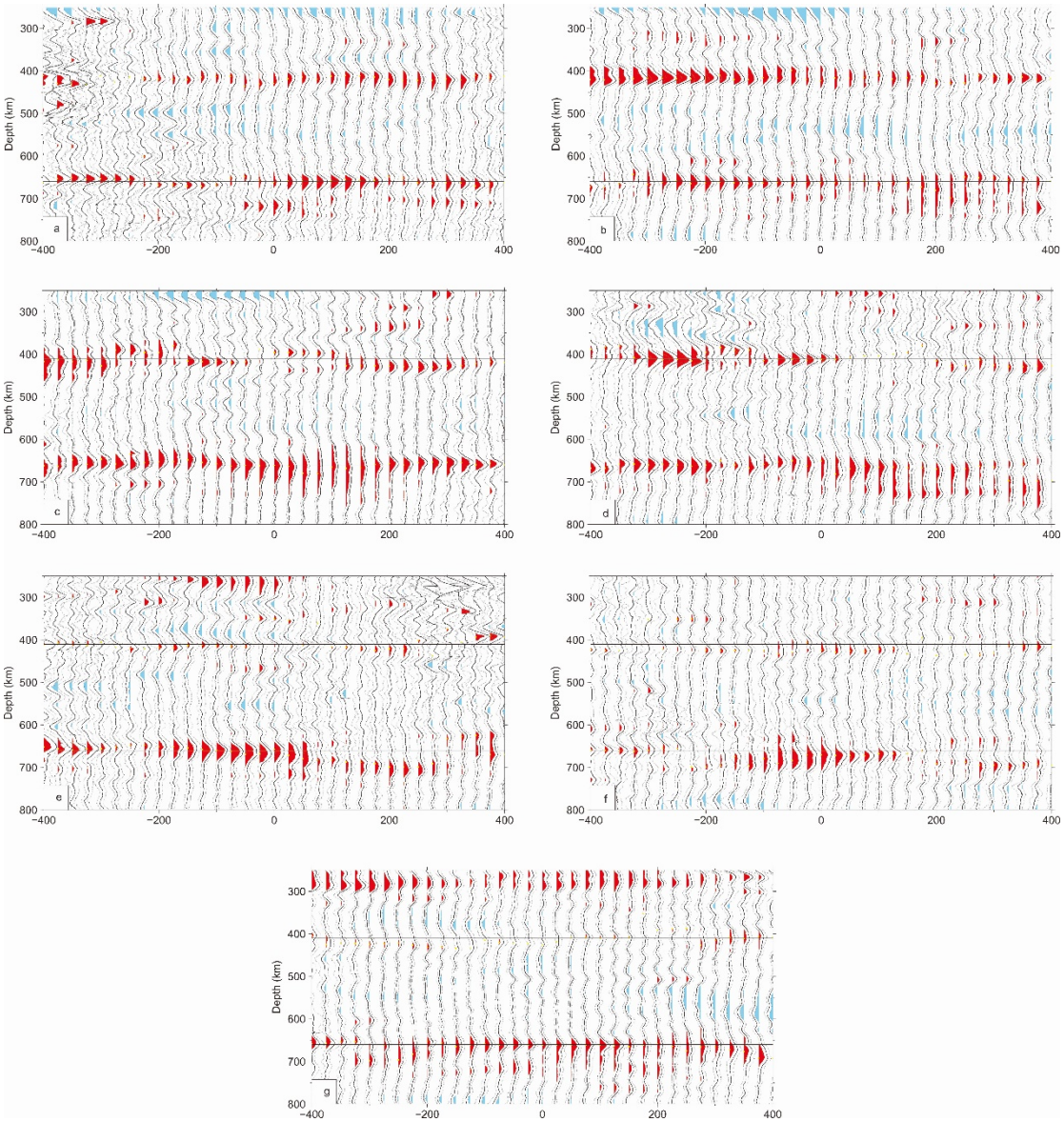

Fig. 4. CCP stacking profiles of receiver functions corrected by a 3-D global P- and S-wave velocity model (Lu et al., 2019). The yellow points we picked for both depths of the 410 km and the 660 km discontinuities on the CCP stacking of receiver functions. The dataset was resampled and calculated with stacked amplitudes 2000 times by employing the bootstrapping method, and the final mean receiver functions corresponding to the 95% confidence level were calculated. Horizontal scale is in km.

Seven CCP stacking profiles of receiver functions were overlapped with P-wave

velocity perturbation profiles (profile location, please see Fig. 1). The results show that the topography of both the 410 and 660 km discontinuities (Fig. 4) is close to the global average depth (Flanagan and Shearer, 1999; Houser et al., 2008). However, the 410 km discontinuity becomes weak or vanishing at e, f and g profiles (Fig. 4e, f and g). We superimpose the CCP stacking profiles on the P-wave perturbation profiles (Fig. 5), the weak and vanishing 410 km discontinuities basically coincide with the high-velocity anomaly (Hv4) (Fig. 5f, g).

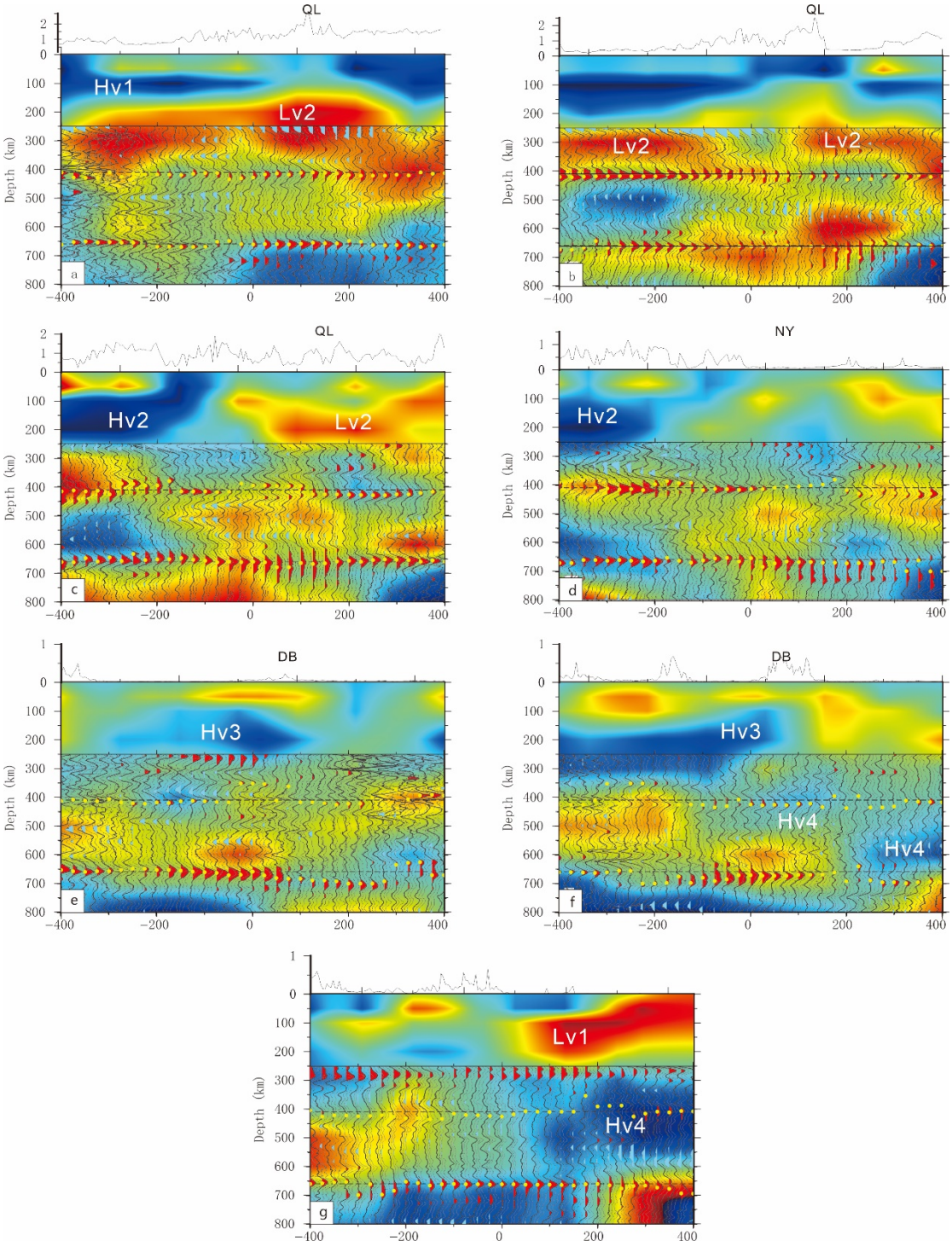
QL
Hv1
Lv2
Depth (km)
a
QL
Lv2
Lv2
b
QL
Hv2
Lv2
c
NY
Hv2
d
DB
Hv3
e
DB
Hv3
Hv4
Hv4
f
Lv1
Hv4
g

Fig. 5. CCP stacking profiles of receiver functions overlain on P-wave perturbation profiles. The yellow points we picked for both the depths of the 410 km and the 660 km discontinuities on the CCP stacking of receiver functions. Horizontal scale is in km.

1. Discussion

The wide occurrence of UHP rocks with diagnostic ultrahigh-pressure mineral assemblages in the DQOB suggests deep subduction and exhumation process (Chang et al., 2021; Deng et al., 2021). However, the results from this study do not indicate the presence of any subducted slab beneath the orogenic belt. He and Zheng (2018) noted that the high-velocity anomalies (Hv2 and Hv3) have a thickness of 200 km, which is much larger than the thickness of either oceanic or continental lithosphere. The Hv2 and Hv3 anomalies may be related to the break-off of the subducted slab.

It is generally believed that the DOB was constructed through continent-continent collision between the NCB and the Yangtze Block (YB) in the Middle to Late Triassic (Hacker et al., 2004) and that the lithosphere of the YB was subducted beneath the NCB to more than 100 km in the upper mantle, leading to a thickened lithospheric root beneath the orogen. The post-magmatic intrusions, heat flow values and geochemical features indicate that the orogenic collapse of the DOB might have occurred in the early Cretaceous (Xu et al., 2007; Zhang et al., 2020), marking the delamination of the lithospheric root and thickened lower crust in this area (He et al., 2011). The Hv2 and Hv3 are horizontal plates rather than blob-shaped subducted slabs, and therefore, these high-velocity anomalies (Hv2 and Hv3) could also represent lithospheric and lower crustal delamination.

Subduction and delamination are major processes that lead to the recycling of crustal materials into the mantle, generating mantle heterogeneities reflected in seismic velocity structure (He, 2020; Stern, 2002; Turner et al., 2017). The ocean-continent subduction in the QOB occurred during Early Paleozoic followed by continent-continent collision along the Shangdan Suture Zone in the Late Paleozoic (Dong et al., 2021). Previous studies suggested that the Silurian-Devonian oceanic crust started subduction during the Late Carboniferous to Early Permian in the DOB (Dong et al., 2021). The subducted slab or delamination of the lower crust an lithosphere can result in partial melting and dehydration of the oceanic crust (Hu et al., 2021; Kelemen et al., 2007; Zheng et al., 2019), as well deep subduction induce return flow of the mantle (Santosh, 2010; Zhao and Ohtani, 2009). In the QOB, the results from our present study reveal a low-velocity anomaly (Lv2) at depths of 200-400 km, which may be related to above deep process. Once the temperature of the low-velocity anomaly (e.g., Lv2) is higher than that of the surrounding mantle, mantle upwelling occurs (Deuss, 2007, Foulger, 2012; Sleep, 2004).

The Hv2 and Hv3 anomalies appear at depths of 200-300 km, where also UHP assemblages are stable. Subsequent mantle upwelling would bring these rocks

to shallower domains and subsequently exhume to the surface.

Our CCP stacking images of receiver function indicate that the topographies of 410 and 660 km discontinuities are close to the global average depth, suggesting that the mantle upwelling might not have originated from the mantle transition zone. If so, this would result in the topography variations of the upper mantle discontinuities (Foulger, 2012). On the other hand, an important finding from this study is that the high-velocity anomaly can induce weak and vanishing 410 km discontinuity, the processes for which require further investigations.

1. Conclusions

Our seismic tomographic studies define plate-shaped high-velocity anomaly at depths of 100-400 beneath the Qinling-Dabie Orogenic Belt, which we correlate with the break-off of the subducted slab or lithospheric and lower crustal delamination. We also define low-velocity anomaly at depths of 200-400 km beneath this orogenic belt.

Based on a detailed analyses of the data obtained in this study, we suggest that the UHP metamorphic rocks in the Qinling-Dabie Orogenic Belt were generated through deep subduction of slab, or lithospheric and lower crustal delamination. It is possible that the exhumation of these rocks from deeper to shallower domains was aided by mantle upwelling.

Acknowledgments

We thank the National Key R&D Plan of China (2017YFC601406). Waveform data for this study were provided by the Data Management Center of the China National Seismic Network at the Institute of Geophysics (Zheng et al., 2010). The raw data involved in CCP stacking of receiver function and tomography can be accessed via https://doi.org/10.5281/zenodo.5118474.

References

Ames, L., Tilton, G.R., Zhou, G., 1996. Geochronology and isotopic character of ultrahigh-pressure metamorphism with implications for collision of the Sino-Korean and Yangtze cratons, central China. Tectonics 15, 472-489.

Boschi, L., Becker, T., Soldati, G., Dziewonski, A.M., 2006. On the relevance of Born theory in global seismic tomography. Geophys. Res. Lett., 33, L06302.

Chai, R., Yang, J., Du, Y., Liu, J. He, F., Huang, Y., Ma, Q., Dai, X., 2020. Constraints on the early Mesozoic denudation of the Qinling orogen from Upper Triassic-Lower Jurassic successions in the Zigui Basin, central China. Journal of Asian Earth Sciences 195, 104360.

Chang, H., Wu, Y., Zhou, G., Zhang, W., He, Y., Zhao, Y., Hu, P., Hu, Z., 2021. Zircon U–Pb geochronology and geochemistry of the Lajimiao mafic complex in the Shangdan Suture Zone, Qinling orogen: Petrogenesis and tectonic mplications. Lithos 390-391, 106113.

Chevrot, S., Sylvnder, M., Diaz, J., Ruiz, M., Paul, A., the PYROPE Working Group, 2015. The Pyrenean architecture as revealed by teleseismic P-to-S-converted waves recorded along two dense transects. Geophys. J. Intern. 200, 1096-1107.

Chopin, C., 1984. Coesite and pure pyrope in high-grade blueschists of the Western Alps: a first record and some consequences. Contrib. Mineral. Petrol. 86, 107-118.

Deng, L.P., Liu, Y.C., Groppo, C., Rolfo, F., Yang, Y., Gu, X.F., Wang, A.D., 2021. New constraints on P-T-t path of high–T eclogites in the Dabie orogen, China. Lithos 384-385, 105933.

Deuss, A., 2007. Seismic observations of transition-zone discontinuities beneath hotspot locations. Geol. Soc. Am. Spec. Pap. 430, 121-136.

Dong, Y., Sun, S., Santosh, M., Zhao, J., Sun, J., He, D., Shi, X., Hui, B., Cheng, C., Zhang, G., 2021. Central China Orogenic Belt and amalgamation of East Asian continents. Gondwana Research, https://doi.org/10.1016/j.gr.2021.03.006.

Dong, S.W., Li, Q.S., Gao, R., Liu, F.T., Xu, P.F., Liu, X.C., Xue, H.M., Guan Y., 2008. Moho-mapping in the Dabie ultrahigh-pressure collisional orogeny, central China. Am. J. Sci. 308, 517-528.

Dong, Y.P., Santosh, M., 2016. Tectonic architecture and multiple orogeny of the Qinling Orogenic Belt, Central China. Gondwana Res. 29, 1-40.

Eagar, K.C., Fouch, M.J. and James, D.E. 2010. Receiver function imaging of upper mantle complexity beneath the Pacific Northwest, United States. Earth Planet. Sci. Lett., 297, 141-153.

Eberhart-Phillips, D., 1986. Three-dimensional velocity structure in Northern California Coast Ranges from inversion of local earthquake arrival times. Bull. Seismol. Soc. Am. 76, 1025-1052.

Efron, B., Tibshirani, R.B., 1986. Bootstrap methods for standard errors, confidence intervals, and other measures of statistical accuracy. Stat. Sci. 1, 54-75.

Flanagan, M.P., Shearer, P.M., 1999. A map of topography on the 410-km discontinuity from PP precursors. Geophys. Res. Lett. 26, 549-552.

Foulger, G.R., 2012. Are 'hot spots' hot spots?. J. Geodyn. 58, 1-28.

Hacker, B.R., Ratschbacher, L., Liou, J.G., 2004. Subduction, collision and exhumation in the ultrahigh-pressure Qinling-Dabie orogen. Geol. Soc. Lond., Spec. Publ. 226, 157-175.

Hacker, B.R., Ratschhacher, L., Webb, L., 1998. U/Pb Zircon ages constrain the architecture of the ultrahigh-pressure Qinling-Dabie Orogen, China. Earth Planet. Sci. Lett. 161, 215-230.

Hansen, P., 1992. Analysis of discrete ill-posed problems by means of the L-curve. *S*IAM Rev. 34, 561-580.

He, C.S., 2020. Upwelling mantle plume and lithospheric delamination beneath the North China Craton. Physics of the Earth and Planetary Interiors 306, 106548.

He, C.S., Dong, S.W., Chen, X.H., Santosh, M., Li, Q.S., 2014. Crustal structure and continental dynamics of central China: a receiver function study and implications for ultra-high pressure metamorphism. Tectonophysics 610, 172-181.

He, C.S., Zheng, Y.F., 2018. Seismic evidence for the absence of deeply subducted continental slabs in the lower lithosphere beneath the Central Orogenic Belt of China. Tectonophysics 723, 178-189.

He, Y., Li, S., Hoefs, J., Huang, F., Liu, S.A., Hou, Z., 2011. Post-collisional granitoids from the Dabie orogen: New evidence for partial melting of a thickened continental crust. Geochim. Cosmochim. Acta 75, 3815-3838.

Houser, C., Masters, G., Shearer, P.M., Laske, G., 2008. Shear and compressional velocity models of the mantle from cluster analysis of long-period waveforms. Geophys. J. Int. 174, 195-212.

Hu, Z., Zeng, L., Förster, M.W., Zhao, L., Gao, L., Li, H., Yang, Y., Li, S., 2021. Recycling of subducted continental crust: Geochemical evidence from syn-exhumation Triassic alkaline mafic rocks of the southern Liaodong Peninsula. Lithos 400-401, 106353.

Jiang, M.M., Ai, Y.S., Chen, L., Yang, Y.J., 2013. Local modification of the lithosphere beneath the central and western North China Craton: 3-D constraints from Rayleigh wave tomography. Gondwana Res. 24, 849-864.

Kelemen, P.B., Hanghj, K., Greene, A.R., 2007. One view of the geochemistry of subduction-related magmatic arcs, with an emphasis on primitive Andesite and lower crust. Treat. Geochem. 3, 1-70.

Kennett, B.L.N., Engdahl, E.R., 1991. Travel times for global earthquake location and phase identification. Geophys. J. Int. 105, 429-465.

Langston, C.A., 1979. Structure under Mount Rainier, Washington, inferred from teleseismic body waves. J. Geophys. Res. 84, 4749-4762.

Lei, J., 2012. Upper-mantle tomography and dynamics beneath the North China Craton, J. Geophys. Res. 117, B06313.

Li, C., van der Hilst, R.D., Toksöz, M.N., 2006. Constraining P-wave velocity variations in the upper mantle beneath Southeast Asia. Phys. Earth Planet. Inter. 154, 180-195.

Li, Y., Liu, Y.C., Yang, Y., Rolfo, F., Groppo, C., 2020. Petrogenesis and tectonic significance of Neoproterozoic meta-basites and meta-granitoids within the

central Dabie UHP zone, China: Geochronological and geochemical constraints. Gondwana Research 78, 1e19.

Liu, L., Liao, X.Y., Wang, Y.W., Wang, C., Santosh, M., Yang, M., Zhang, C.L., Chen, D.L., 2016. Early Paleozoic tectonic evolution of the North Qinling Orogenic Belt in Central China: Insights on continental deep subduction and multiphase exhumation. Earth Sci. Rev. 159, 58-81.

Lu, C., Grand, S.P., Lai, H., Garnero, E.J., 2019. TX2019slab: A New P and S Tomography Model Incorporating Subducting Slabs. J. Geophys. Res. 124, 11549-11567.

Luo, Y.H., Xu, Y.X., Yang, Y.J., 2012. Crustal structure beneath the Dabie orogenic belt from ambient noise tomography. Earth Planet. Sci. Lett. 314, 12-22.

Ma, Q., Yang, J., Du, Y., Dai, X., Chai, R., Guo, H., 2021. Yajun Xu Early Triassic initial collision between the North China and South China blocks in the eastern Qinling Orogenic Belt. Tectonophysics 814, 228965.

Niu, P.P., Jiang, S.Y., 2021. Geochemistry, zircon U–Pb geochronology, and Hf isotopes of the metavolcanic rocks in the Tongbai orogen of central China: Implication for Neoproterozoic oceanic subduction to slab break-off. Precambrian Research 361, 106239.

Okay, A.I., Xu, S.T., Sengor, A.M.C., 1989. Coesite from the Dabie Shan eclogites, central China. Eur. J. Mineral. 1, 595-598.

Paige, C., Saunders, M.L., 1982. SQR: an algorithm for sparse linear equations and sparse least squares. Assoc. Comput. Math. Trans. Math. Software 8, 43-71.

Okay, A.I., Xu, S.T., Sengor, A.M.C., 1989. Coesite from the Dabie Shan eclogites, central China. Eur. J. Mineral. 1, 595-598.

Santosh, M., 2010. Assembling North China Craton within the Columbia supercontinent: The role of double-sided subduction. Precambrian Res. 178, 149-167.

Schneider, F.M., Yuan, X., Schurr, B., Mechie, J., Sippl, C., Haberland, C., Minaev, V., Oimahmadov, I., Gadoev, M., Radjabov, N., Abdybachaev, U., Orunbaev, S., Negmatullaev, S., 2013. Seismic imaging of subducting continental lower crust beneath the Pamir. Earth Planet. Sci. Lett. 375, 101-112.

Shen, W.. Ritzwoller, M.H., Kang, D., Kim, Y.H., Lin, F.C., Ning, J. Wang, W., Zheng, Y., Zhou, L., 2016. A seismic reference model for the crust and uppermost mantle beneath China from surface wave dispersion. Geophy. J. Int. 206, 954-979.

Shi, W., Chen, L., Chen, X., Cen, M., Zhang, Y., 2019. The Cenozoic tectonic evolution of the faulted basins in the northern margin of the Eastern Qinling

Mountains, Central China: Constraints from fault kinematic analysis. Journal of Asian Earth Sciences 173, 204-224.

Sleep, N.H., 2004. Thermal haloes around plume tails. Geophys. J. Int. 156, 359-362.

Smith, D.C., 1984. Coesite in clinopyroxene in the Caledonides and its implications for geodynamics. Nature 310, 641-644.

Sobolev, N.V., Shatsky, V.S., 1990. Diamond inclusions in garnets from metamorphic rocks; a new environment of diamond formation. Nature 343, 742-746.

Stern, R.J., 2002. Subduction zones. Rev. Geophys. 40, 1012.

Tian, Y., Zhao, D., 2013. Reactivation and mantle dynamics of North China Craton: insight from P-wave anisotropy tomography. Geophys. J. Int. 195, 1796-1810.

Turner, S.J., Langmuir, C.H., Dungan, M.A., Escrig, S., 2017. The importance of mantle wedge heterogeneity to subduction zone magmatism and the origin of EM1. Earth Planet. Sci. Lett. 472, 216-228.

VanDecar, J.C., Crosson, R.S., 1990. Determination of teleseismic relative phase arrival times using multi-channel cross-correlation and least squares. Bull. Seismol. Soc. Am. 80, 150-169.

Wei, W., Zhao, D., Xu, J., Zhou, B., Shi, Y.L., 2016. Depth variations of P-wave azimuthal anisotropy beneath Mainland China. Scientific Reports 6, 29614.

Xu, H., Ma, C., Ye, K., 2007. Early cretaceous granitoids and their implications for the collapse of the Dabie orogen, eastern China: SHRIMP zircon U–Pb dating and geochemistry. Chem. Geol. 240, 238-259.

Xu, M.J., Huang, H., Huang, Z.C., Wang, P., Wang, L.S., Xu, M.J., Mi, N., Li, H., Yu, D.Y., Yuan, X.H., 2018. Insight into the subducted Indian slab and origin of the Tengchong volcano in SE Tibet from receiver function analysis. Earth Planet. Sci. Lett. 482, 567-579.

Xu, S.T., Okay, A.I., Ji, S.Y., Sengor, A.M.C., Su, W., Liu, Y.C., Jiang, L.L., 1992. Diamond from the Dabie Shan metamorphic rocks and its implication for tectonic setting. Science 256, 80-82.

Wang, C.Y., Zeng, R.S., Mooney, W.D., Harker, B.R., 2000. A crustal model of the ultrahigh-pressure Dabie Shan orogenic belt, China, derived from deep seismic refraction profiling. J. Geophys. Res. 105B, 10857-10869.

Wang, X.M., Liou, J.G., Mao, H.K., 1989. Coesite-bearing from the Dabie Mountains in central China. Geology 17, 1085-1088.

Wu, Y.B., Zheng, Y.F., 2013. Tectonic evolution of a composite collision orogen: An overview on the Qinling-Tongbai-Hong'an-Dabie-Sulu orogenic belt in central China. Gondwana Res. 23, 1402-1428.

Yang, B.J., Mu, S.M., Jin, X., Liu, C., 1996. Synthesized study on the geophysics of Manzhouli-Suifenhe geoscience transect, China. Acta Geophysica Sinica 39, 772-782.

Yang, F., Xue, F., Santosh, M., Wang, G., Kim, S.W., Shen, Z., Jia, W., Zhang, X., 2019. Late Mesozoic magmatism in the East Qinling Orogen, China and its tectonic implications. Geoscience Frontiers 10, 1803e1821.

Yuan, X.C., Klemperer, S.L., Teng, W.B., Liu, L.X., Chetwin, E., 2003. Crustal structure and exhumation of the Dabie Shan ultrahigh-pressure orogen, eastern China, from seismic reflection profiling. Geology 31, 435-438.

Zhang, A., Guo, Z., Afonso, J.C., Yang, Y., Yang, B., Xu, Y., 2020. The deep thermochemical structure of the Dabie orogenic belt from multiobservable probabilistic inversion. Tectonophysics 787, 228478.

Zhao, D., Hasegawa, A., Horiuchi, S., 1992. Tomographic imaging of P- and S-wave velocity structure beneath northeastern Japan. J. Geophys. Res. 97, 19909-19928.

Zhao, D., Hasegawa, A., Kanamori, H., 1994. Deep structure of Japan subduction zone as derived from local, regional and teleseismic events. J. Geophys. Res. 99, 22313-22329.

Zhao, D., Ohtani, E., 2009. Deep slab subduction and dehydration and their geodynamic consequences: evidence from seismology and mineral physics. Gondwana Res. 16, 401-413.

Zhao, L.R., Allen, M., Zheng, T., Zhu, R., 2012. High-resolution body wave tomography models of the upper mantle beneath eastern China and the adjacent areas. Geochem. Geophys. Geosyst. 13, Q06007.

Zhao, L., Paul, A., Guillot, S., Solarino, S., Malusà, M.G., Zheng, T.Y., Aubert, C., Salimbeni, S., Dumont, T., Schwartz, S., Zhu, R.X., Wang, Q.C., 2015. First seismic evidence for continental subduction beneath the Western Alps. Geology 43, 815-818.

Zheng, Y.F., Xiao, W.J., Zhao, G.C., 2013. Introduction to tectonics of China. Gondwana Res. 23, 1189-1206.

Zheng, Y.F., Xu, Z., Chen, L., Dai, L.Q., Zhao, Z.F., 2019. Chemical geodynamics of mafic magmatism above subduction zones. J. Asian Earth Sci. 104185.

Zheng, Y.F., Zhou, J.B., Wu, Y.B., Xie, Z., 2005. Low-grade metamorphic rocks in the Dabie-Sulu orogenic belt: A passive-margin accretionary wedge deformed during continent subduction. Intern. Geol. Rev. 47, 851-871.

Zhu, L. and Kanamori, H. 2000. Moho depth variation in southern California from teleseismic receiver functions. J. Geophys. Res. 105, 2069-2980.